J. Membrane Biol. 7, 88–110 (1972)

Model Approaches for Evaluation of Cell Coupling in Monolayers

J. SIEGENBEEK VAN HEUKELOM*, J. J. DENIER VAN DER GON, and F. J. A. PROP

Medical Physics Department, Physical Laboratory, State University of Utrecht, Utrecht, The Netherlands, and Pathological-Anatomy Laboratory, University of Amsterdam, Amsterdam, The Netherlands

Received 17 September 1971

Summary. The electrical coupling of epithelial cells of the intestine of chick embryo cultured in monolayers was studied. This coupling can be evaluated by regarding the monolayer as a honeycomb structure of cells and the cells as equipotential spaces, as long as the cells are small (diameter <25 μm). With help of this discrete model it was found that for the non-junctional membrane the membrane resistance is $\varrho_m = 250 - 2{,}000\ \Omega\ \text{cm}^2$, and for the junctional membrane $\varrho_i = 5 - 50\ \Omega\ \text{cm}^2$. In addition to this discrete model, a continuous model was also considered and good agreement between the two descriptions was found. With the aid of the continuous model, a value for the non-junctional membrane capacitance (C_m) was obtained: $5 - 50\ \mu\text{F/cm}^2$. The electrical values are not corrected for membrane folding, microvilli and the like. Tentative corrections based on electron microscopy suggest: $1{,}000 < \varrho_m < 10{,}000\ \Omega\ \text{cm}^2$, $10 < \varrho_i < 100\ \Omega\ \text{cm}^2$, $1 < C_m < 10\ \mu\text{F/cm}^2$.

Coupling of cells by low-resistance junctions is a commonly accepted phenomenon. It has been demonstrated in a number of different cell systems: epithelial tissue (Loewenstein, 1966; Furshpan & Potter, 1968), embryonic cells (Ito & Hori, 1966; Potter, Furshpan & Lennox, 1966; Furshpan & Potter, 1968; Sheridan, 1968; Ito & Loewenstein, 1969), heart (Weidmann, 1966, 1970; Mendez, Mueller & Urguiaga, 1970), smooth muscle (Tomita, 1970), tissue culture (Furshpan & Potter, 1968; Hyde, Blondel, Matter,

* *Present address:* Department of Animal Physiology, University of Amsterdam, Amsterdam, The Netherlands.

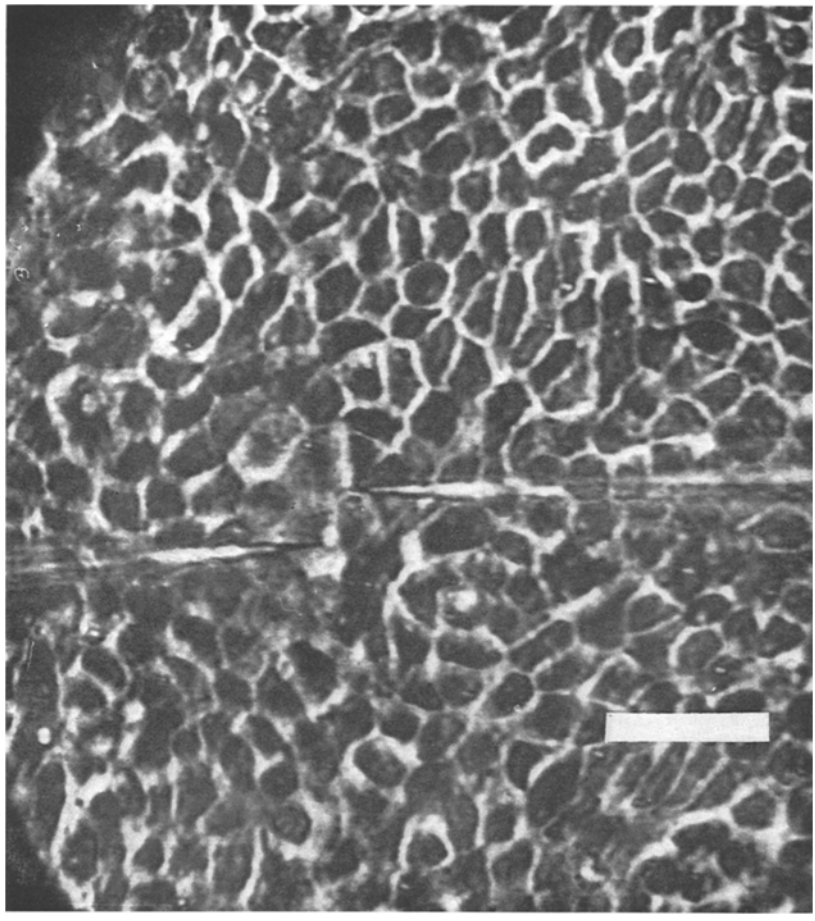

Fig. 1. Photograph of monolayer with two microelectrodes (bar = 50 μm)

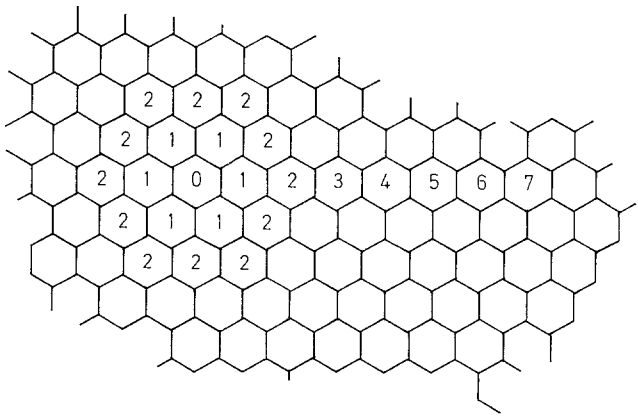

Fig. 2. Honeycomb idealization of the monolayer: order numbers are indicated

Cheneval, Filloux & Girardier, 1969; Borek, Higashino & Loewenstein, 1970; O'Lague, Dalen, Rubin & Tobias, 1970; Siegenbeek van Heukelom, Denier van der Gon & Prop, 1970), plant cell systems (Spitzer, 1970), nerve cell synapses (Furshpan & Potter, 1959; Bennet, 1966; Furshpan, 1964; Walker & Hild, 1969) and some other cell systems (Penn, 1966; Revel & Sheridan, 1968); a useful review is given by Loewenstein (1968).

This paper deals with the quantitative estimation of the electrical properties (specific resistance and capacitance) of the membranes in one cell system: a monolayer of cells freshly cultured from chick embryo intestinal epithelium. The main features of it are its easy access for microelectrodes under microscopic control and its favorable physiological state. No proteolytic enzymes were used in its preparation and the interval between explantation and measurement was as short as possible (3 days), thereby reducing the hazard of artifacts due to subculturing.

With the help of common electrophysiological methods, the electrotonic spread in the monolayer cell system has been determined as well as the input resistance of the system. For evaluation of these and other quantities, the configuration of the cell system has to be taken into account. A reasonable approximation is a honeycomb (Figs. 1 and 2), a model in which there is close packing of the cells, each having six neighbors. An approximate analysis of our idealized model is given in the next section. A few other discrete models were also considered, and gave only slightly different results.

In general, the junctional membranes show low resistances, compared to the resistances of the non-junctional membranes. Therefore, a continuous model is also discussed in which the junctional membrane resistances are included in the intracellular fluid resistance. This model is compared with the discrete models.

It also provides a basis for the evaluation of the specific membrane capacitance of the non-junctional membrane.

Finally, the cell monolayers were studied by electron microscopy to obtain more information on the geometry of the cell membranes and on possible sites of high conductance in the junctional membranes.

Materials and Methods

Cell Cultures

When starting these experiments the authors considered treatment of the cells with proteolytic enzymes to be unfavorable, and a technique was used where this treatment was not needed. Lately, the work of Borek *et al.* (1970) has demonstrated cell coupling

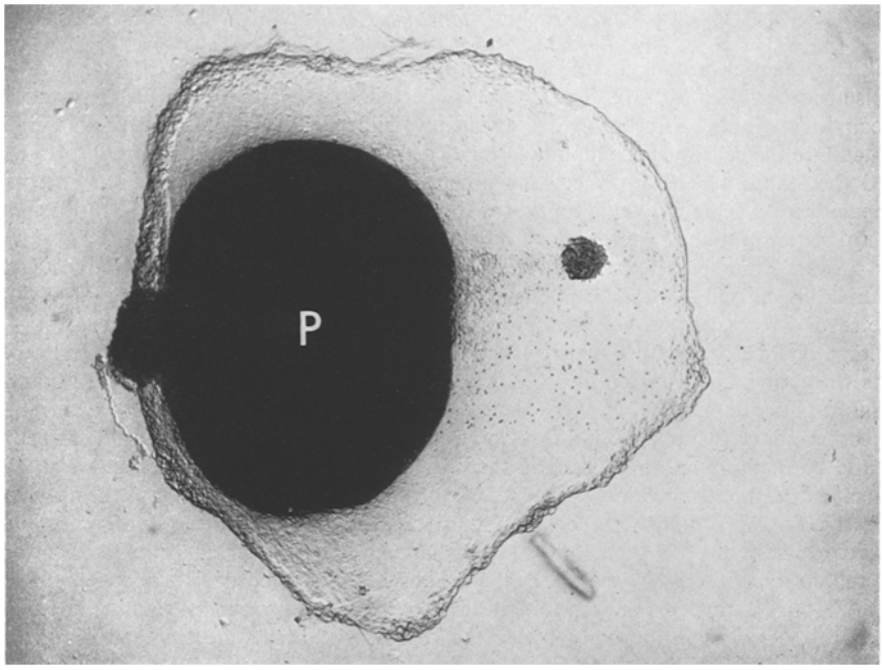

Fig. 3. Photograph of explant (diameter of the original explant), the black patch (*P*), about $\frac{1}{2}$ mm

in sheets of cells that have been treated with trypsin. But, the method of culturing described by us can be regarded as providing layers of cells with a physiological state as near as possible to the *in vivo* state.

Newly fertilized hens' eggs were incubated at 38 °C for 10 days. The embryos were removed from the eggs under sterile conditions. The small intestines were taken out and transfered to a petri dish; a drop of cultivation medium (*see* below) was added to prevent drying out.

It proved essential to free the intestinal tubes very carefully from the attached mesenterial mesenchyme by means of fine-tipped scalpels (surgical blades no. 11); if not freed thus, the cultures were overgrown by fibroblasts. The intestinal tubes were cut into pieces about 0.3 mm long. These were placed in Leighton tubes (Bellco no. 1962) on glass cover slips moistened with culture medium. The cover slips were new and thoroughly cleaned by means of repeated washing with ethanol before sterilization. After about 1 hr, just enough culture medium (0.5% lactalbumine hydrolysate, 20% calf serum in Hank's saline) was added to submerge the cover slip, leaving the tissue fragments protruding through the fluid surface. The surface tension served to anchor the explants until they became attached. After 18 hr, enough medium could be added to cover the explants. The culture medium was renewed every 24 hr. In the course of 3 days, large sheets of coherent intestinal epithelium grew around the explants from most of the pieces (Fig. 3). Cell migration, as well as cell division, was observed in these sheets.

Sometimes penicillin was added to prevent infection.

Experimental Set-Up

The microelectrodes were glass micropipettes filled with 3 M KCl having a d–c-resistance of 40 to 70 MΩ. They were connected to the amplifiers (Keithley 605) by means of a Hanks' solution bridge and a reversible electrode (Ag–AgCl) and were inserted into the cells by micromanipulation. The input resistance at insertion (7 to 15 MΩ) and the stability of the intracellular potential (−20 mV) were criteria for successful impalement. The actual value found for the intracellular potential appeared to be a less useful criterion than its stability.

Electrotonic spread was measured with two electrodes: one electrode injected the stimulating current (I_{stim}: a symmetrical square wave at 3 Hz, between 10^{-9} and 10^{-8} A); the second recorded the voltage changes in different cells. After initially recording the voltage change a certain distance from the current electrode, the recording electrode was withdrawn and inserted into the next cell toward the current electrode. In this way a more or less complete potential distribution in the monolayer could be determined. Injection and measurement were made with respect to a reversible electrode immersed in the bath. Stimulation was made through a 5 GΩ resistor; precautions were taken to safeguard the rectangularity of the waveform. The cut-off frequency of the amplifiers was 3 kHz. Recordings of the stimulating current and the voltage differences were made by means of a UV oscillograph with a bandwidth of 3 kHz (e.g., Fig. 8). Recordings of the resting potential were made by means of a penrecorder (bandwidth 0.5 Hz).

The stimulating current, ten times attenuated, was used for measuring the resistances of both electrodes inside and outside the cells; resistances were frequently measured to follow possible changes in their values.

The bathing fluid was continuously refreshed; it consisted of Hank's saline (Oxoid) with 10% calf serum added.

With the microelectrodes in place (Fig. 1), the microscope field was photographed after each measurement to verify the distance between the impaled cells. Also, after a series of measurements, a number of surveying pictures were made to judge the location of the measured cells. Measurements were accepted only when the monolayer met the following criteria:

(1) the cells appeared healthy;

(2) the cells were far away from boundaries and irregularities in the monolayer that could disturb the uniform electrotonic spread; and

(3) there was homogeneity in cell configuration.

Insertion of the second electrode is often accompanied by a dip in the record from the electrode impaled first, but no relation between the dip and the measured electrotonic spread could be found.

After making the electrical measurements, the height h of the cells in the part of the monolayer investigated was estimated by taking advantage of the fact that irregular voltage fluctuations are produced by the microelectrode when it touches a surface, either that of the cover slip or the cell. When the tip of the microelectrode was clearly visible through the microscope, this measuring procedure could be followed. The specimen stage was adjusted so that the microelectrode just touched the cell surface at first, and then, consecutively, touched the cover slip at two locations lateral to the monolayer; the height of the specimen stage was read every time it was adjusted. This procedure was repeated several times. From the two measurements on the glass, the height of the glass under the cell was obtained by averaging, taking into account the different locations. From this value, and the one found on top of the cell surface, the height of the cell was found. Finally, the monolayer was moved horizontally under a microelectrode adjusted

to the top of the cell surface as a check on possible excessive irregularities in the height of the monolayer near the measured cell. The diameter of the cells (parallel to the glass) was measured from the micrographs.

Theory and Analysis

A. The Discrete Model

Because of the mathematical treatment of the results, it will be useful to consider the analysis first.

The starting point of the analysis is the idealization to a honeycomb structure as illustrated in Fig. 2, with the following assumptions: (1) All cells have equal heights (h) and equal sides (d); (2) the contribution of the resistivity (Ω cm) of the intracellular and extracellular fluid is negligible with respect to the resistance contributions of the junctional and non-junctional membranes; (3) the specific membrane resistances ($\Omega\,\mathrm{cm}^2$) are supposed to be independent of the transmembrane voltages; (4) the cells can be considered as ordered in rings around a central cell with order number zero which contains the stimulating electrode; and (5) there are no current leaks through the membranes on the underside of the monolayer, or the junctional gap between the cells.

Throughout this paper, specific resistances are used as defined, because these are thought to be more easily related to electron microscopic findings than resistances defined in other ways. Besides, they are probably less dependent on the geometry of the whole cell.

The number of the cells in each ring is

$$N_m = 6m \text{ (with } N_0 = 1), \tag{1}$$

m being the number assigned to the rings.

The length of the border between rings with order number m and $m+1$ is

$$L_m = 6(2m+1)d. \tag{2}$$

The projected upper surface of one cell is

$$S_c = \tfrac{3}{2} d^2 / \sqrt{3} \tag{3}$$

while the surface of one ring is

$$S_m = N_m \cdot S_c. \tag{4}$$

If it is assumed that the cells in one ring have equal potentials (V_m), there are three currents associated with one ring due to the current injected by the stimulating electrode: $i_{1,m}$ the current entering from the ring with

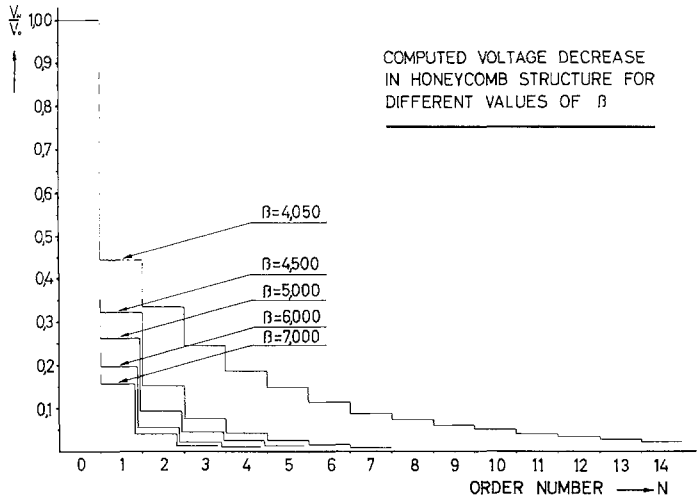

Fig. 4. Influence of $\beta(\beta=4+\delta)$ upon the electrotonic spread in the discrete model

order number $m-1$; $i_{2,m}$ the current flowing to the ring with order number $m+1$; $i_{3,m}$ the current leaking to the bath. The potential in the bathing fluid is taken as zero. The specific complex conductances (specific admittances) of the junctional and non-junctional membranes are g_i and g_m, respectively. With Kirchhoff's first law $i_{1,m}=i_{2,m}+i_{3,m}$, one obtains:

$$m\beta V_m=(2m-1)\,V_{m-1}+(2m+1)\,V_{m+1} \tag{5}$$

with

$$\beta=4+\frac{3}{2}\sqrt{3}\,\frac{d}{h}\,\frac{g_m}{g_i}. \tag{6}$$

For $m=0$, one has

$$i_0=I_{\text{stim}}=g_i\,6\,d\,h(V_0-V_1)+g_m\tfrac{3}{2}\sqrt{3}\,d^2\,V_0. \tag{7}$$

Another boundary condition is

$$V_m=0 \quad \text{for } m\to\infty. \tag{8}$$

By neglecting the membrane capacitances (steady state), one obtains

$$\beta=4+\frac{3}{2}\sqrt{3}\,\frac{d}{h}\,\frac{\rho_i}{\rho_m} \tag{9}$$

where ρ_i is the specific membrane resistance of the junctional membrane, and ρ_m is the specific resistance of the non-junctional membrane.

$\delta=\beta-4$ is the factor defining cell coupling. It equals the ratio between the resistance (R_i) of the membrane between two adjacent cells and the resistance of the non-junctional membrane of one cell (R_m), and contains a

geometrical factor d/h, as well as the ratio between the specific resistances of the junctional and non-junctional membranes ρ_i/ρ_m.

By introducing the specific membrane capacitances one gets: $g_m = sC_m + 1/\rho_m$ and $g_i = sC_i + 1/\rho_i$ with $s \equiv d/dt$. The parameter C_i is difficult to obtain experimentally. Because of the low values for R_i in comparison with R_m, only very large values of C_i would be detectable. This is not likely, and was not found.

Eq. (5), with boundary conditions [Eqs. (7), (8) and (9)], can be solved with a computer, taking $V_0 = 1$ and approximating Eq. (8) with $V_m = 0$ with m large (for instance, $m = 100$), (*see* Fig. 4). Fitting the values found in this way to the data, one can evaluate V_0, V_1 and δ. Eqs. (7) and (9) then yield values for ρ_i and ρ_m[1].

The choice $C_m \neq 0$ made the program rather extensive and was not tried.

B. The Continuous Model

Results evaluated with the help of the discrete model indicated a rather low ρ_i compared with ρ_m. This suggested that a continuous model, in which the specific junctional membrane resistance is included in the intracellular resistivity, would hold rather well (a similar approach has been followed by Hyde *et al.*, 1969). In this case, the introduction of a time dependent term ($C_m \neq 0$), and the solution of the resulting equation, is relatively simple. The electrotonic spread now obeys the Laplace equation:

$$\frac{\partial^2 V}{\partial R^2} + \frac{1}{R}\frac{\partial V}{\partial R} - V = \frac{\partial V}{\partial T} \tag{10}$$

with the dimensionless quantities

$$R = r(\rho_v/\rho_m h)^{\frac{1}{2}} = r/\lambda, \tag{11}$$

$$T = t/C_m \rho_m = t/\tau \tag{12}$$

and ρ_v the resistivity (Ω cm) of the monolayer, including the resistance of the junctional membranes; r is the distance from the current-carrying

1 Dr. J. Strackee directed our attention to the fact that Eq. (5) can be solved with the help of the method of Laplace. Taking $V_0 = 1$, the general solution is

$$V_n = K^{-1}(m^2) \int_0^{\pi/2} \left\{ \frac{m^n \sin^{2n}\phi}{\sqrt{1 - m^2 \sin^2\phi}} \right\} d\phi.$$

It follows that $V_1 = k\left\{1 - \frac{E(k^2)}{K(k^2)}\right\}$ with $k = \beta/4 - \left(\frac{\beta^2}{16} - 1\right)^{\frac{1}{2}}$, $K(k^2)$ the complete elliptic integral of the first kind and $E(k^2)$ the complete elliptic integral of the second kind (Abramowitz & Stegun, 1964). The values for $V_n (n = 2, 3, \ldots)$ are easily computed with the help of V_0, V_1 and the recurrent relation Eq. (5).

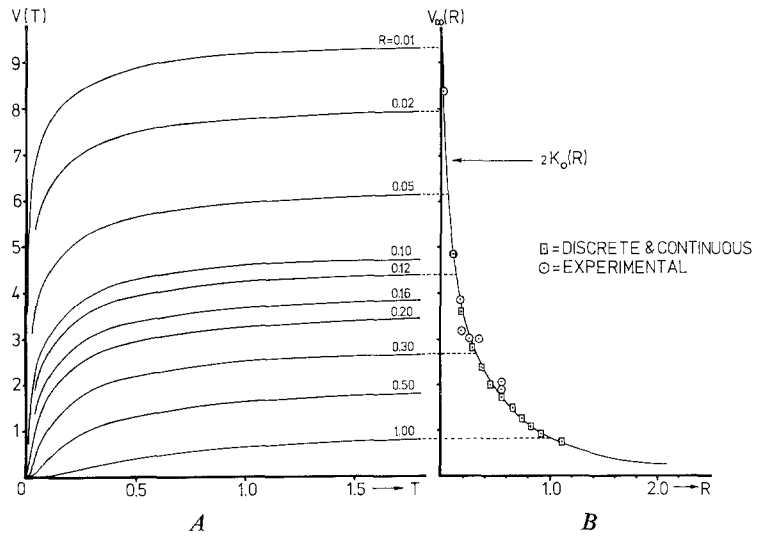

Fig. 5. (*A*) Relation between $V(R, T)$ and T for several relevant values of R, as obtained by numerical computation of Eq. (15). (*B*) $2K_0(R)$; ⊡: Results obtained by the discrete model and the continuous model (Column V and VI of Table 2 and Discussion C). ⊙: Results from series 1-8-'69 (NC) and 3-4-'70*b* fitted to the correct value V_1

electrode; $\lambda=(\rho_m h/\rho_v)^{\frac{1}{2}}$ is called the space constant, and $\tau=C_m\rho_m$ is called the time constant.

A particular solution of the equation is the source solution,

$$w(R, T)=\frac{1}{4\pi T}\exp-\left(\frac{R^2}{4T}+T\right), \tag{13}$$

demonstrating the impulsive response of the model to a current pulse

$$\int_0^\infty w(R, T)\,2\pi R\,dR=e^{-T}. \tag{14}$$

For a step in current (I) one obtains:

$$V(R, T)=V_0\int_0^T w(R, \theta)\,d\theta. \tag{15}$$

V_0 is a multiplicative factor and does not influence the results as all results are taken relative to values V for $T=\infty$ (the stationary state). The value V_0 is found by applying Kirchhoff's first law to the whole monolayer for $T=\infty$. The found value is $V_0=I\rho_v/h$. In Fig. 5 it is taken to be 1. However, the integral needs more attention since it is easily proved with it that from the rise of the voltage records the specific capacity of the non-junctional membrane can be obtained. In transforming the integral, with

$\eta = \pi/2 - 2$ arctg $2\,\theta/R$, it is changed into

$$V(R, T) = \frac{I\rho_v}{4\pi h} \int_{\pi/2 - 2\,\mathrm{arctg}(2T/R)}^{\pi/2} \{\cos^{-1}(\eta) \exp(-R\cos^{-1}\eta)\}\, d\eta. \qquad (15a)$$

From (15a) it follows that, in a time $T = T_{\frac{1}{2}} = R/2$, the induced potential at a distance R has risen to half its final value. It therefore follows that:

$$R/2 = T_{\frac{1}{2}} = t_{\frac{1}{2}}/C_m \rho_m = r(\rho_v/4\rho_m h)^{\frac{1}{2}}. \qquad (16)$$

By putting $2\,\theta/R = \exp(x)$ it can be easily proved that for $T = \infty$, Eq. (15), apart from the constant V_0, is identical with $2K_0(R)$, the modified Bessel function of the second kind. The substitution leads to an integral representation of K_0 (Abramowitz & Stegun, 1964) (*see* Fig. 5*B*). This agrees with the continuous solution of the steady state potential distribution.

C. Transition from the Discrete Model to the Continuous Model

In the honeycomb structure, two repeating rectangular units can be found (Fig. 6). The lengthwise resistance of each unit, divided by its length and multiplied by its width and height, gives an overall resistivity value

$$\rho_v = \rho_c + \rho_i/d\sqrt{3}, \qquad (17)$$

in which ρ_c represents the resistivity of the cytoplasm. These repeating units serve as unit cells for estimating ρ_v, and the computed result is correct in 12 directions in the monolayer. This fact, in view of the irregularities in the real monolayer, suggests that this value is a reasonable approximation for all directions in the monolayer.

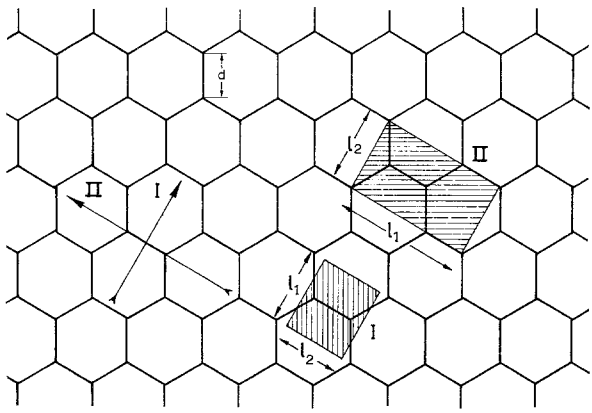

Fig. 6. Repeating rectangular unit cells in the monolayer

Eq. (11) with Eq. (17) gives:

$$R = r\left(\frac{\rho_c}{h\rho_m} + \frac{2\delta}{9d^2}\right)^{\frac{1}{2}}. \tag{18}$$

With ρ_c of the order $10^2\ \Omega$ cm [a value normally found in electrophysiological work (*see* Schanne, 1969)] it is clear that in our case, $\rho_c \ll \rho_i/(d\sqrt{3})$ holds (*see* Table 1); therefore,

$$\rho_v \simeq \rho_i/d\sqrt{3} \quad \text{and} \quad R \simeq \frac{r}{3d}\cdot(2\delta)^{\frac{1}{2}}. \tag{17a) (18a}$$

The specific membrane capacitance follows from (16) and (18a):

$$C_m = 6t_{\frac{1}{2}}\, d/\rho_m r(2\delta)^{\frac{1}{2}}. \tag{19}$$

As the electrode distance r is not measured, but the order number of the cells with respect to each other is, r should be replaced by the mean radius Q_m of the ring with this order number. This mean radius is approximately equal to $r_m = 1.6\,dm$ (*see* Discussion and Table 2). But, since measuring in the ring of order number m includes the whole ring, and not only the portion to its center, a discontinuity correction seems appropriate; $r = 1.6\,d(m+\frac{1}{2})$ was therefore used in the transition from the discrete to the continuous model. Besides, with this correction, better consistency has been obtained in a series of values of C_m, as calculated from the experimental results.

Results

A. Linearity

The analysis presented here is based on the assumption that the membrane resistance is independent of the transmembrane voltage.

A test of this assumption is given in Fig. 7, which shows a linear relation between stimulating current and the induced voltage in the first-order cell. The linear relation agrees with the linear difference of Eq. (5). But this result should be considered with caution. Many membranes with different transmembrane voltages contribute to the result, and linearizing effects may certainly play a role, as has been shown by Noble (1962, 1966).

B. Time Course

To verify whether the general shape of Fig. 5 is correct, a few measurements were made with the help of an averaging computer (C.A.T.) connected to the output of the amplifiers. In this way the noise level could be reduced

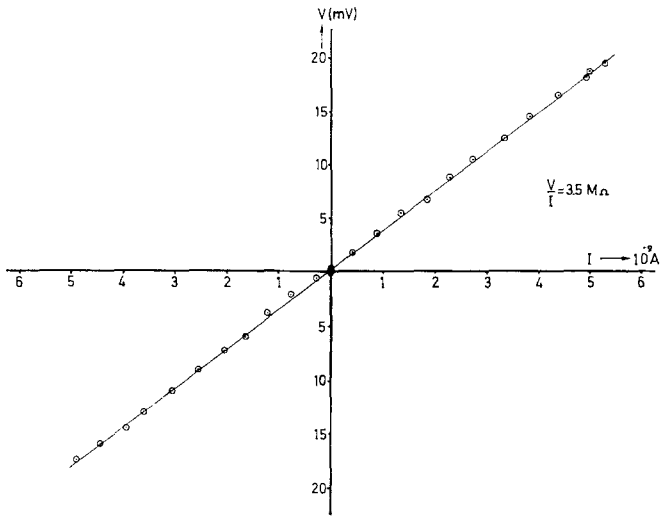

Fig. 7. Linearity test: the voltage in the first-order cell V_1 as a function of the injected current I_{stim}

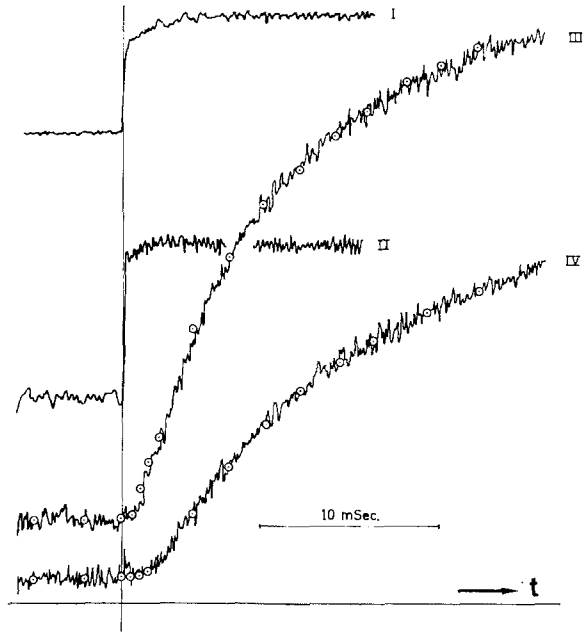

Fig. 8. Average current steps (I and II, addition of 100 records) and voltage changes in cells with order number 2 and 5, respectively. III (addition of 205 records) and IV (addition of 215 records). Time resolution: 0.2 msec. Inserted are points obtained from the solution of Eq. (15), with $R=0.30$ and $R=0.80$, respectively

and the actual shape of the step response [Eq. (15)] could be studied rather well. Results are illustrated in Fig. 8. The points inserted in the figure are obtained from the solution of Eq. (15); $T_{\frac{1}{2}}$ [*see* Eq. (16)] is chosen in such a way that a good fit was obtained. There is reasonable agreement with the shape predicted theoretically. The current records (I and II) do not correspond exactly to a step function, but resemble it well enough.

C. Other Results

The results are compiled in Table 1. The figures in column VI, the average membrane potential $\overline{V}_M$, are obtained directly from the measurements. This is also true for the figures in columns IV and V, except for the top two in both columns (series '69). With these first two series, not much attention was given to the exact values of d and h, and the figures mentioned have to be considered as rough estimates. Column XIV gives an average of the actual rise times, divided by $m+\frac{1}{2}$, as described in the analysis. Column III contains a number of remarks concerning the way some corrections were carried out. "Manipulated" (M) means that both $t_{\frac{1}{2}}$ and V_m gave a better fit with an order number different than the one observed. If the microscopic photographs did not give conclusive evidence to the contrary, this new order number was used (*see* also Discussion B). "Corrected" (C) means that a correction was introduced for deviation of the measured potential V_M from the average membrane potential $\overline{V}_M$. Possible causes are: leakage near the electrodes, and disturbance due to nearby cells, which were impaled already. The corrected induced potential was computed with

$$V_m(\text{after correction}) = V_m \frac{\overline{V}_{M,S} \cdot \overline{V}_{M,R}}{V_{M,S} \cdot V_{M,R}}, \tag{20}$$

where V_m is the measured value for electrotonic spread, $V_{M,S}$ is the membrane potential measured with the stimulating electrode, $V_{M,R}$ is the membrane potential measured with the recording electrode, $\overline{V}_{M,S}$ is the membrane potential $V_{M,S}$ averaged over the series and $\overline{V}_{M,R}$ is the membrane potential $V_{M,R}$ averaged over the series. Averaging was done over the entire series of cells which were impaled for the purpose of characterizing the potential field.

Column VII shows the values of δ which best fit the model computations with the measured results. Also, from this best fit, best values of V_0 and V_1 can be obtained (columns VIII and IX give these values when I_{stim} was

Table 1

I Series no.	II Measured cell orders	III Remarks	IV d (μm)	V h (μm)	VI $\overline{V_M}$ (mV)	VII δ	VIII V_0 (mV)	IX V_1 (mV)	X ϱ_m (Ωcm^2)	XI ϱ_i (Ωcm^2)	XII ϱ_v (kΩcm)	XIII λ (μm)	XIV $t_{\frac{1}{2}}/m+\frac{1}{2}$ (msec)	XV τ (msec)	XVI C_m (μF/cm^2)
1-8-'69 *	0, 1, 2, 3, 6	NC/M	8	9	31	0.012	43	24	1,600	8.2	5.9	155	0.6	14	9
		C/M				0.061	74	36	600	16	12	74		7	10
3-9-'69	1, 2, 3	NC	8	9	22	0.0002	48	33	70 k	6.3	4.5	1,200	1.7	310	4
		C				0.034	210	108	3 k	44	25	92		24	8
20-3-'70*a* *	0, 1, 2	NC	7.3	9.6	14.5	0.35	175	61	270	48	40	26	1.7	7	27
		C				0.70	170	50	140	50	40	18		5	37
20-3-'70*b*	0, 1, 3, 5	NC	8.7	11.4	25	0.20	169	58	670	66	45	42	1.2	7	11
		C				0.0014	74	45	24 k	17	11	490		85	3
3-4-'70*aP*	0, 1, 3, 4	NC	8.5	8.5	18	0.35	87	29	190	25	17	31	3.5	16	83
		C				0.065	59	28	540	13	9.1	71		35	67
3-4-'70*b* *	1, 2, 4, 6	NC	7.9	8.0	20.5	0.022	78	42	1,600	14	10	113	0.6	10	6
		C				0.022	64	35	1,300	11	8.0	113		10	8
25-5-'70 *	1, 3, 4	NC	7.2	7.2	21	0.035	104	54	1,200	16	13	81	1.5	21	16
		C				0.088	121	59	600	19	15	51		13	23
4-9-'70 *	0, 1, 4, 7	NC	6.1	5.6	6.4	0.078	105	49	380	11	11	46	2.1	20	53
		NC/M				0.055	114	56	600	12	11	55		24	40
		C/M				0.055	87	42	470	11	11	55		24	43

Table with measured and computed results. In column I, an asterisk after the series number means that this series is used in the averaging, as mentioned in Discussion A; *P* means that this series was measured very near to the original patch (*see* Fig. 3). In column III NC = not corrected, C = corrected and M = "manipulated" (*see* Results and Discussion A), d = length of the hexagon-side, h = height of the monolayer, $\overline{V_M}$ = average membrane potential during the series, V_0 and V_1 are the potentials due to electrotonic spread obtained from the measured values with the found value of δ, and $I_{\text{stim}} = 10^{-8}$ A was used as the starting point for the other results; ϱ_m is calculated with Eqs. (7) and (9); ϱ_i is calculated with the same equations; ϱ_v is calculated with Eq. (17a); λ with $\lambda = 3d/(2\delta)^{\frac{1}{2}}$; $t_{\frac{1}{2}}$ is $t_{\frac{1}{2}}(m)/m+\frac{1}{2}$; τ and C_m are calculated with Eqs. (12) and (19).

taken as $I=10^{-8}$ Å). With the help of Eqs. (7) and (9), ρ_m and ρ_i can be computed (columns X and XI). Next, ρ_v can be computed [Eq. (17a), column XII], and from these values the space constant λ is found (column XIII). Finally C_m and τ can be computed with Eqs. (12) and (19) [columns XVI and XV]. The symbols added to column I are discussed in Discussion A.

Discussion

A. Discussion of Table 1

Some criteria can be given for selecting the values of Table 1 which are the most reliable. First, there should be enough measurements in cells with different order number to give a reasonable series.

Second, the variance of the membrane resting potentials V_M in a series of measurements may be used as an indication of the functional homogeneity of the monolayer and the success of penetrations. One possibility is to omit a measurement if the stimulated or the explored cell has too extreme a membrane potential. Another possibility is to try to correct for deviating membrane potentials. For instance, if a leak is present as a result of the impalement or other causes, the membrane potential, as well as the measured electrotonic spread, will drop to lower values. A correction of the electrotonic spread according to Eq. (20) may be carried out. The results obtained in this way did turn out to be more consistent. Sometimes, only the corrected values gave reasonable results.

Our measure of cell communication δ turned out to be very sensitive even to small corrections. As these corrections relate the results to the stability of V_M it seems sensible to require that δ (before correction) should not differ too much from the value of δ obtained after correction and that it should be at least the same order of magnitude.

Examples where these criteria are not met, are the series 3-9-'69 and 20-3-'70*b* showing what, in fact, can occur.

Average results of series which meet the above mentioned criteria are, if given on the basis of the non-corrected results (averaging carried out over the results marked with an asterisk): $\rho_m=1{,}000\ \Omega\ \mathrm{cm}^2$, $\rho_i=20\ \Omega\ \mathrm{cm}^2$, $\rho_v=15\ \mathrm{k}\Omega\ \mathrm{cm}$, $\lambda=85\ \mu\mathrm{m}$ and $C_m=21\ \mu\mathrm{F/cm}^2$. On the basis of the corrected results one finds: $\rho_m=620\ \Omega\ \mathrm{cm}^2$, $\rho_i=21\ \Omega\ \mathrm{cm}^2$, $\rho_v=17\ \mathrm{k}\Omega\ \mathrm{cm}$, $\lambda=60\ \mu\mathrm{m}$ and $C_m=24\ \mu\mathrm{F/cm}^2$. The average for V_M is $\bar{V}_M=19\ \mathrm{mV}$. It should be stressed that these average values only give an impression of the average values of parameters of all the monolayers.

That the measured results may represent measured differences from one monolayer to the other is illustrated with series 3-4-'70*aP* (*see* also Fig. 3). This series is measured a few cells away from the original explant patch; thus different results could be expected.

It is remarkable that with low values of $\bar{V}_M$ (4-9-'70) measured communication is as good as when $\bar{V}_M$ is high. In most cases, the impalement introduced some structural change in the cell, resulting in a change in the darkness of the cell as observed by the phasecontrast microscope (*see* Fig. 2). Usually, the onset of this darkening is *not* related to a change in V_M. Often the cell regained its normal appearance a short time after the electrode was retracted. More often than not, a low V_M coincided with difficulties with the impalement and a very slow (if any) recovery of the cell after impalement. The reason for these observations and their relation to our results is rather obscure.

Not derived in the analysis is the relation between λ and δ, which is, [with Eqs. (9), (11) and (17a)], $\lambda^2 \delta = 9d^2/2$, so λ and δ both serve as a measure of cell coupling quite well. When, for instance, $R_i = R_m$, then $\delta = 1$, $\lambda \approx 2d$ (here this would be 15 μm) and $V_1/V_0 = 0.2$. With values more representative of our results, $\rho_i : \rho_m \approx R_i : R_m = 1:50$, and therefore $\delta = 1/50$, $\lambda \approx 125$ μm and $V_6/V_0 = 0.2$.

In the first case, the cell may be considered to be isolated. In the second case, 5 rings (≈ 100 cells) are more or less acting together with a 100-fold buffering capacity. In general, the buffering capacity will be sufficiently represented by either R_m/R_i, or δ^{-1} or λ^2.

B. Some Preliminary Electron Microscopic Findings

Some preliminary results of an electron microscopic investigation of the structure of these cell sheets can be presented. These results come from perpendicular and frontal sections of cell sheets grown on mica.

The cells overlap like roof tiles, but the abutting surfaces show an intricate pattern of contact areas (Fig. 9).

In frontal sections, large desmosome-like structures are seen (*see* Fig. 10).

The total area of cell contact between two adjacent cells is certainly larger than the area derived from the measurement of d and h (*see* Materials and Methods). What part of the junctional complex serves as the low-resistance path between the cells can not be decided from the results obtained. The cells, however, can be regarded as equipotential spaces (*cf.*

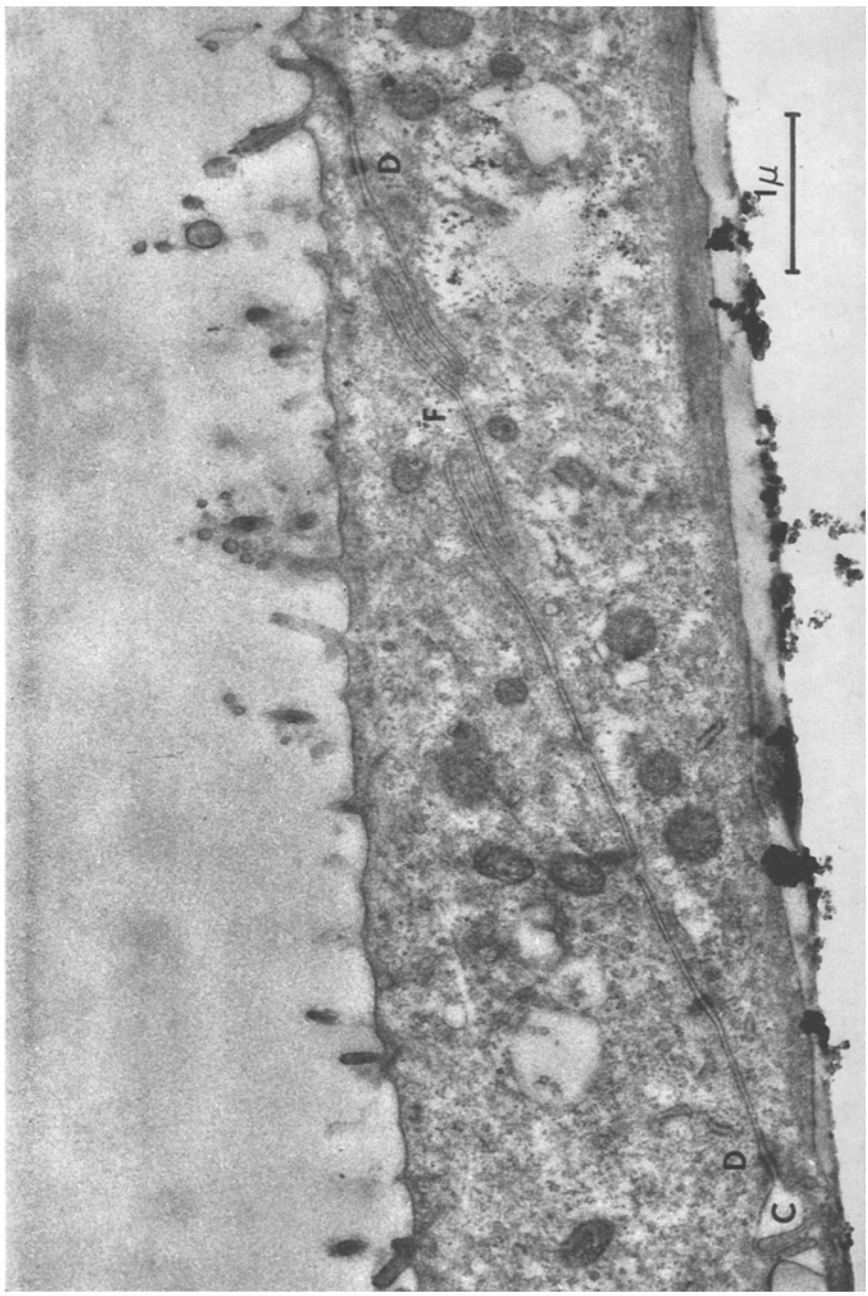

Fig. 9. Section perpendicular to the cell sheet. The contact region between two cells shows an intricate pattern of desmosomes (*D*) interdigitating pattern (*F*) with closely parallel cell membranes and cavernous parts (*C*). The upper cell surface is studded with small villi. A space of about 0.1 μm remains between the lower cell surface and the substrate (mica). Particles of India ink at the lower surface of the embedded cell sheet marked regions of interest for sectioning

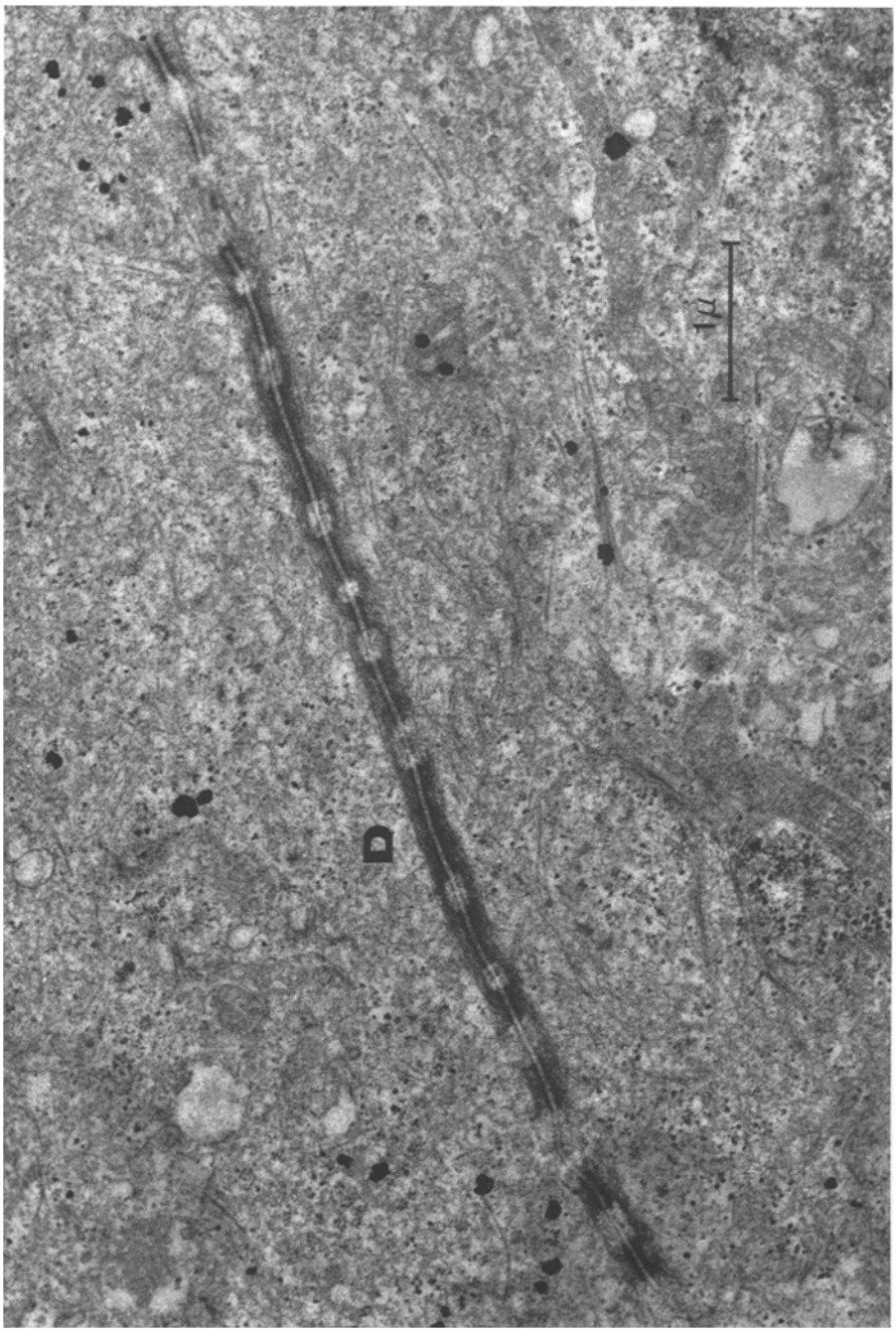

Fig. 10. Frontal section of cell sheet at the region of cell contact showing a serial ordering of desmosomes with small interspaces

Analysis C) and only a form factor needs to be introduced to relate the actual low-resistance area to the area assumed by us (*dh*). Unfortunately, no electron microscopy was carried out on the cells of the series in Table 1.

The upper surface of the cells is studded with microvilli (Fig. 9). The height of the microvilli is about 0.5 μm and their diameter about 0.1 μm. Up to 20 of these microvilli are found per μm^2. In this way, the surface area is increased up to 4 times. Some spread in the resistance and capacitance of the non-junctional membrane (ρ_m and C_m, respectively) is justified by these findings. Besides, if one takes this enlarged surface area into account, the actual membrane capacitance is reduced to more acceptable values. Tentative estimates for ρ_m, ρ_i and C_m are: $1{,}000 < \rho_m < 10{,}000\ \Omega\ cm^2$, $10 < \rho_i < 100\ cm^2$, $1 < C_m < 10\ \mu F/cm^2$.

The height of the cells measured from the electron micrographs (2 to 3 μm) does not agree with the height measured according to the method described in Materials and Methods (8 to 9 μm) (*see* Table 1). This difference is very much larger than the shrinkage of the cells perpendicular to the substrate, which, as may be expected from current fixation and embedding methods, do not exceed 20%. For electron microscopic work the cells were grown on thin micasheets, whereas for the electrophysiological work the cells were usually grown on cover glasses. In regard to the electrical measurements, no differences were found between the two substrates. A possible explanation for the difference in height is that these preliminary electron micrographs were not made from the same monolayer in which the electrophysiological measurements were made. Also other parts of monolayers may have been used for the electron micrographs than the parts where analogues to the electrophysiological measurements were made. Finally, the roof-tile overlap of the cells may have been the reason for the inaccurate attribution of order numbers. A small space was found between the undersurface of the cells and the mica. This was possibly present between the glass and the cells during the measurements. The influence of this space can easily be evaluated in two extreme situations: the space acts either as an insulator, or as a pool in free contact with the bathing fluid. In the first case, the results remain as given. In the second case, all values for the specific resistances of the non-junctional membranes should be multiplied by two, and the specific capacities divided by two. [Compare the difference between Eq. (1) and Eq. (10) in the article of Hyde *et al.*, 1969]. A more complicated situation between these two extremes is conceivable, with an intricate pattern of leakage paths between the cells, from the underside to the upperside of the monolayer. The stationary state analysis will still hold, but the time response will be changed and will influence the results. This could be

an explanation for the rather high values found for the specific capacities of the non-junctional membranes.

C. The Honeycomb Structure

One of the starting points of the analysis is the assumption of a honeycomb structure in which cells with equal order number (i.e., belonging to the same ring) show equal potentials. This assumption is clearly not correct since cells in the corners of the hexagonal rings are in a different situation, with respect to the central one, than the cells in the middle of the hexagon-sides. Because of the irregularities in the monolayer, however, the different relation of cells in one ring to the central cell is much less distinct than in the honeycomb structure. Idealizations with other shapes of cells can be introduced. For ring-like models, with square or segment-like cells, one can derive formulas similar to Eq. (5) but with different constants in δ representing the different idealizations. The differences found between these different idealizations do not exceed 15%.

To test the assumption of the honeycomb structure in our monolayers, the number of cells (N_1) surrounding one cell was counted in photographs similar to Fig. 2; N_1 ranged from 3 to 9. A frequency distribution of the results is shown in Fig. 11 ($F_{0,t}$ as a function of N_1). It shows a sharp peak for $N_1 = 6$ (mean 6.07). Mean values found for the number of cells in the second and third ring were 12.8 and 19.8, respectively.

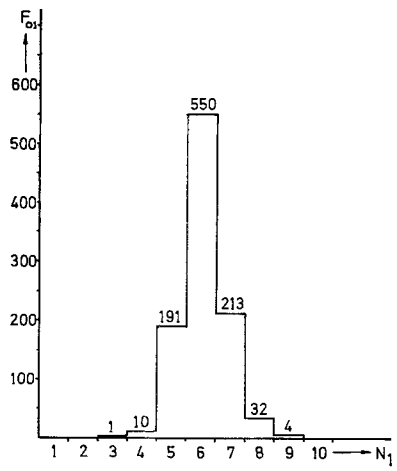

Fig. 11. Frequency histogram of the cells in the monolayer with respect to the number of their neighbors

Table 2

I m	II $Q_m = r_m/d$	III Q_m/m	IV R ($\delta = 0.015$)	V $(V_m/V_1)_D$	VI $(V_m/V_1)_C$
1	1.732	1.732	0.100	1.000	1.000
2	3.232	1.616	0.187	0.743	0.746
3	4.890	1.630	0.282	0.593	0.591
4	6.355	1.589	0.367	0.489	0.491
5	7.927	1.585	0.458	0.412	0.410
6	9.502	1.584	0.549	0.352	0.350
7	11.078	1.583	0.640	0.304	0.302
8	12.655	1.582	0.731	0.264	0.260
9	14.233	1.581	0.822	0.230	0.227
10	15.811	1.581	0.913	0.202	0.197
11	17.389	1.581	1.004	0.178	0.174
12	18.967	1.581	1.095	0.157	0.153

Table for evaluation of the transition of the discrete model to the continuous model. m is the order number; $Q_m = r_m/d$ is the average distance of cell centers in the model of a ring, with order number m, to the center of the zero order cell with respect to the hexagon side d; Q_m/m is the same value divided by the cell order number m; $R = Q_m(2\delta)^{\frac{1}{2}}/3$ is the corresponding distance in the continuous model [Eq. (18a)]. The columns V and VI are the computed values V_m in relation to V_1 in the discrete (D) and the continuous model (C). The results are shown graphically in Fig. 5*B*.

Comparison of the discrete model with the continuous one is of special interest, as both models have their advantages. The mean ring radius Q_m of the m-th ring with respect to d [$Q_m = r_m/d$] is given in Table 2, with r_m computed from the model (column II). Also the mean ring radius divided by m, thus Q_m/m, is given (column III), which turns out to be approximately 1.6. The continuous model predicts a potential distribution given by $2K_0(R) = 2K_0(r/\lambda)$, with R in the m-th ring corresponding with $Q_m(2\delta)^{\frac{1}{2}}/3$ [Eq. (18a) and column IV]. Finally, computed values V_m/V_1 for the discrete, as well as for the continuous model, are given in Table 2 (columns V and VI) and Fig. 5*B* assuming $\delta = 0.015$; in the figure some normalized values from experiments are also given (*see* also Siegenbeek van Heukelom *et al.*, 1970). The agreement is satisfactory.

We wish to thank Dr. P. F. Elbers for the electron micrographs and for his comments, Martha Kreunen and Miriam de Jong-Lutz for preparing the cultures, Ank van Wees for her assistance and Thijs Zoethout for the computer programming.

References

Abramowitz, M., Stegun, I. A. 1964. Handbook of Mathematical Functions, National Bureau of Standards, Washington D.C.

Bennet, M. V. L. 1966. Physiology of electrotonic junctions. *Ann. N.Y. Acad. Sci.* **137**:509.

Borek, C., Higashino, S., Loewenstein, W. R. 1970. Intercellular communication and tissue growth: IV: Conductance of membrane junctions of normal and cancerous cells in culture. *J. Membrane Biol.* **1**:274.

Furshpan, E. J. 1964. "Electrical transmission" at an excitatory synapse in a vertebrate brain. *Science* **144**:878.

Furshpan, E. J., Potter, D. D. 1959. Transmission at the giant motor synapses of the crayfish. *J. Physiol.* **145**:289.

Furshpan, E. J., Potter, D. D. 1968. Low resistance junctions between cells in embryos and tissue culture. *Current Topics in Devel. Biol.* **3**:95.

Hyde, A., Blondel, B., Matter, A., Cheneval, J., Filloux, J. P., Girardier, L. 1969. Homo- and heterocellular junctions in cell cultures. *Progr. Brain Res.* **31**:283.

Ito, S., Hori, N. 1966. Electrical characteristics of *Triturus* egg cells during cleavage. *J. Gen. Physiol.* **49**:1019.

Ito, S., Loewenstein, W. R. 1969. Ionic communication between early embryonic cells. *Devel. Biol.* **19**:228.

Loewenstein, W. R. 1966. Permeability of membrane junctions. *Ann. N.Y. Acad. Sci.* **137**:441.

Loewenstein, W. R. 1968. Communication through cell junctions. Implications in growth control and differentiation. *J. Devel. Biol. Suppl.* **2**:151.

Mendez, C., Mueller, W. J., Urguiaga, X. 1970. Propagation of impulses across Purkinje fiber-muscle junctions in dog heart. *Circulation Res.* **26**:135.

Noble, D. 1962. The voltage dependence of the cardiac membrane conductance. *Biophys. J.* **2**:381.

Noble, D. 1966. Applications of Hodgkin Huxley equations to excitable tissues. *Physiol. Rev.* **46**:1.

O'Lague, P., Dalen, H., Rubin, H., Tobias, C. 1970. Electrical coupling: Low resistance junctions between mitotic and interphase fibroblasts in tissue culture. *Science* **170**:464.

Penn, R. D. 1966. Ionic communication between liver cells. *J. Cell. Biol.* **29**:171.

Potter, D. D., Furshpan, E. J., Lennox, E. S. 1966. Connections between cells of the developing squid as revealed by electrophysiological methods. *Proc. Nat. Acad. Sci.* **55**:328.

Revel, J. P., Sheridan, J. D. 1968. Electrophysiological and ultrastructural studies of intercellular junctions in brown fat. *J. Physiol.* **194**:34P.

Schanne, O. F. 1969. Measurement of cytoplasmic resistivity by means of the glass microelectrode. *In:* Glass Microelectrodes. M. Lavallée, O. F. Schanne and N. C. Hébert, editors, p. 299. John Wiley and Sons, Inc., New York.

Sheridan, J. D. 1968. Electrophysiological evidence for low resistance intercellular junctions in the early chick embryo. *J. Cell. Biol.* **37**:650.

Siegenbeek van Heukelom, J., Denier van der Gon, J. J., Prop, F. J. A. 1970. Epithelial monolayers: A study object for cell communication. *Biophys. Biochem. Acta* **211**:98.

Spitzer, N. C. 1970. Low-resistance connections between cells in the developing anther of the lily. *J. Cell. Biol.* **45**:565.

Tomita, T. 1970. Electrical properties of mammalian smooth muscle. *In:* Smooth Muscle. E. Bülbring, A. F. Brading, A. W. Jones, and T. Tomita, editors. p. 197. William Clowes and Sons, London.

Walker, F. D., Hild, W. J. 1969. Neuroglia electrically coupled to neurons. *Science* **165**:602.

Weidmann, S. 1966 The diffusion of radiopotassium across intercalated disks of mammalian cardiac muscle. *J. Physiol.* **187**:323.

Weidmann, S. 1970. Electrical constants of trabecular muscle from mammalian heart. *J. Physiol.* **210**:1041.